Correlation between native As$_2$Se$_3$ preform purity and glass optical fiber mechanical strength

Sylvain Danto [*], Marion Dubernet [1], Baptiste Giroire [1], J. David Musgraves, Peter Wachtel, Thomas Hawkins, John Ballato, Kathleen Richardson

School of Materials Science and Engineering/COMSET, Clemson University, 91 Technology Drive, Anderson, SC 29625, USA

A B S T R A C T

Based on their mid-infrared transparency and tailorable thermo-mechanical properties, chalcogenide glass optical fibers have found numerous technological useful applications in the fields of optic and sensing. However they tend to suffer from mechanical limitations as compared to more conventional oxide-glass fibers, which impede their further integration into components where high strength is required. Reported here are findings on the mechanical properties of fibers based on the glass As$_2$Se$_3$, with a focus on unraveling how extrinsic impurities embedded in the native preform impact the maximum stress that the resulting fibers can endure. Preforms were prepared and subjected to four levels of purification (standard moisture removal, surface oxide volatilization, and synthesis over AlCl$_3$ getter, followed by distillation) and subsequently drawn into fibers. To effectively decouple the real effect of impurity content on fibers strength from other peripheral parameters, such as manufacturing, handling or aging, each purification protocol was duplicated on one bare fiber and one fiber drawn with a protective coating. Weibull statistics on the strength of As$_2$Se$_3$ fibers were determined in both tension and bending. We demonstrate that coated and uncoated fibers follow a similar trend with purification. Specifically, oxide volatilization treatment increases the fibers resistance to failure, while the addition of AlCl$_3$ getter in the melt without subsequent distillation degrades it. If further distillation is carried out the fibers strength improves only slightly as compared to oxide volatilization treatment alone. These results provide both insights into the interplay between chemical, optical, and mechanical properties as well as practical steps benefiting the continued utility of these glass optical fibers.

© 2013 Elsevier Ltd. All rights reserved.

1. Introduction

Chalcogenide glass (ChGs) optical fibers have undergone tremendous development since the mid-1960s [1]. They now are employed in numerous devices applicable to the fields of IR light-wave propagation [2], supercontinuum generation [3,4], medical endoscopy [5], all-optical switching [6], Raman gain engineering [7,8], and fiber-based chemical sensor devices [9], to name just a few. However their use in existing and new applications demands higher mechanical robustness, concurrently with low optical loss; these two attributes together have yet to be achieved. This is in part due to the intrinsically weaker average bond strength of ChG constituents, as compared with oxides glasses. Extrinsic parameters overlap to further reduce ChG-based fibers from their optimal level. For example, multiple flaws at the fibers surface can severely lower their measured strength, the size and density of these imperfections governing, on a "weakest link" model [10,11], the stress level leading to fiber failure. Thus, the fibers survivability is extremely sensitive to practical factors such as manufacturing, handling, storage, or exposure to corrosive environments.

Engineering mechanically-robust, reliable fibers necessitates the use of materials with high intrinsic bond strength and connectivity. A great deal of research has been conducted to better understand how the glass morphology and composition affect its fracture behavior [12–17]. Yet the reported strength of fibers in ChG family remains about one order of magnitude lower than their theoretical value [14]. The mechanical properties of ChGs fibers have also been extensively studied as a function of aging or post-drawing annealing treatment, coating treatment, or drawing parameters [13–16]. However, to the best of our

knowledge, no systematic investigation of the impact of glass purity on fiber strength has been carried out. In the present effort we propose to do so by examining how extrinsic impurities in preforms and fiber mechanical robustness relate to each other. Indeed it has been demonstrated that extrinsic impurities within ChGs matrix can behave as possible crystallite nucleating sites that can alter the thermo-mechanical and/or optical behavior of glass [18–22]. Furthermore it is expected that impurities will have a direct influence on the fiber strength by potentially degrading the glass matrix connectivity. Fiber processing can exacerbate the nucleation and growth of such scattering centers, as the glass is subjected to a robust thermal treatment to achieve a proper draw tension. Impurities in ChGs are mostly in the form of hydrogen, oxygen or carbon compounds that bond with the chalcogen or glass-former constituents [22]. Their concentrations strongly depend on the quality of the initial components and on their subsequent melt processing, the fabrication of high-purity ChGs still remaining challenging.

Recently the authors have evaluated the impact of bulk glass purification, with treatments encompassing oxide removal by thermal treatment, and synthesis over impurity-getters followed by distillation, and quantified the impact of each on resulting physical and optical properties [23]. Investigated here is the dependence of native preform transparency, and associated extrinsic impurities content, on the resulting fibers strength. Macroscopic performs with different levels of purification have been fabricated, drawn into meters-long lengths of fiber, and their strength measured, both in tension (assessing tensile strength) and in bend (compressive) modes. Based on its known thermal stability against crystallization, the canonical stoichiometric As_2Se_3 was selected for this study. In addition to good fiberization ability, it has a high transmittance in the spectral range 2–16 μm, and can be fabricated with moderately low loss (74 dB/km at 4.7 μm [24]). Furthermore, in order to remove any external fiber damage from the actual strength measurements, each purification protocol has been duplicated as follows: the first preform was drawn as-is, while the second one was covered with a UV-cure coating to minimize manufacturing-, handling- or aging-related degradation. Micro-hardness and transparency of the preforms has been correlated with the micro-hardness and strength of their respective fibers. Finally, Weibull statistical analysis of the fiber's strength probability distribution have been applied to the mechanical failure as a function of purification method, both in tensile and in bending.

2. Experimental

2.1. Preform synthesis and purification

Preforms for subsequent fiber drawing are cylindrical glass rods of 35 g in mass, 10 mm in diameter and approximately 10 cm in length. They were produced by the co-fusion of the adequate raw elements, in the appropriated amounts, under vacuum in quartz reaction tubes. The melt was rocked at T_m in a rocking furnace to ensure melt homogeneity and then was rapidly quenched in air. All syntheses were carried out using high-purity starting reagents (As: Alfa Aesar 5 N, Se: Alfa Aesar 5 N). Provided below are the different purifications protocols followed [23].

2.1.1. Moisture removal

The elements As and Se were weighed in a glove-box under nitrogen atmosphere and batched into a silica tube. The reaction tube then was brought under vacuum (10^{-3} mm Hg). Moisture was removed from the reagents and reaction vessel surfaces by holding the system under dynamic vacuum at 100 °C for 4 h. The reaction tube then was sealed using a gas-oxygen torch and inserted into a

rocking electrical furnace at 750 °C for 12 h. In order to improve the homogeneity of the melt, and of the resulting preform, the rocking was stopped following homogenization and the temperature was lowered to 550 °C for 4 h. The tube then was rapidly air-quenched and returned to the furnace for annealing at 180 °C for 2 h.

2.1.2. Oxide volatilization by thermal treatment

Oxide volatilization relies on the large difference in vapor pressure between the pure Se and As elements and their respective oxides (SeO_2 and As_2O_3) to yield dissociation and preferential volatilization of surface oxide contamination. Commercial reagents were introduced into two dry and clean silica tubes, which then were evacuated under dynamic-vacuum (10^{-3} mm Hg). The selenium and arsenic materials were heated for 2 h at 250 °C and 290 °C, respectively, to remove the contaminating surface oxides. Additionally, the procedure also favors the elimination of moisture from the batch. Following this purification, the purified elements were combined in the final silica tube, which was sealed and placed in the rocking furnace for the melting as noted above.

2.1.3. Aluminum tri-chloride getter

Although the thermal treatment described above efficiently removes most volatile oxide impurities, supplementary purification steps were applied to scavenge impurities even further. The first technique involves melting of the glass components over a getter material, which will form thermodynamically stable compounds with residual hydrogen and/or oxygen atoms left in the precursor materials. In this work, $AlCl_3$ was selected as the getter material, which is added in small amounts (0.1% wt) to the reagents during the batching. The Cl^- anions bond with the hydrogen atoms to form a volatile chloridic acid. In the meantime the aluminum is expected to getter the oxygen impurities in the melt to form alumina (Al_2O_3).

2.1.4. Static distillation

The synthesis over the $AlCl_3$ getter usually is followed by a static distillation of the glass to separate the As_2Se_3 material from impurity-containing residues such as the alumina components. The distillation starts by transferring the melted glass into a new silica ampoule designed with two distinct physical sections. The multi-chamber tube then was evacuated, sealed and inserted in a four-zone furnace, with the zones held at 750, 725, 400 and 350 °C, respectively to form a thermal gradient. The chalcogenide, originally located in the 'warmer' zone, vaporizes and condenses in the 'cooler' section of the tube, whereas the higher temperature residue remains behind in the initial zone of the tube. The distilled As_2Se_3 material was then melted again in a clean and dry silica tube to ensure its complete homogeneity.

2.2. Fiber drawing

The preforms were drawn using a 6.5-meters-high optical fiber draw tower (Clemson University), as schematically depicted in Fig. 1a. The draw tower is composed of an annular electrical furnace with a sharp temperature profile, a diameter monitor, a tension dancer and a collecting drum among other pieces of control and data measurement instruments. The heating chamber is maintained under continuous dry nitrogen gas flow (0.5 l/min) to avoid oxidation of the surface of the preform during the fiber processing. The preform, inserted into the translating holder, can be seen in Fig. 1b. It is held at the top of the tower and slowly fed into the furnace. The temperature is gradually increased at a rate of 5 °C/min to ~350 °C to locally soften the bottom-section of the preform, until forming a drop which fell down initially by gravity. The preform-holder motion and capstan rotation velocity were
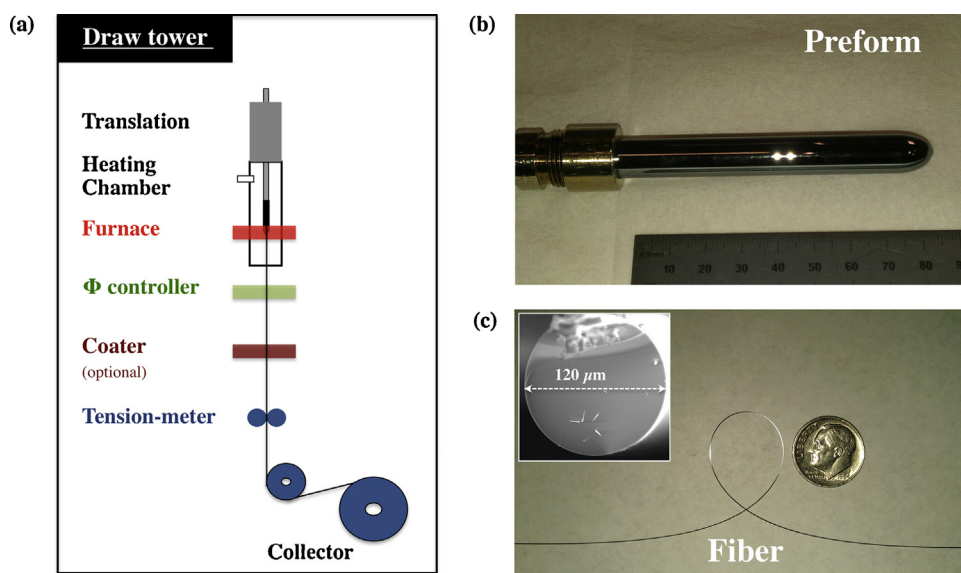
Fig. 1. (a) Draw tower schematic, (b) As_2Se_3 glass preform inserted into its holder and (c) As_2Se_3 fiber (inset: SEM micrograph of the cross-section of an uncoated fiber).

controlled in real-time to produce the targeted fiber diameter. Following this procedure, many meters of fibers were drawn with diameters ranging from 250 μm, down to 75 μm (Fig. 1c; inserted: SEM micrograph of a fiber cross-section).

When required, a UV-cureable polymer coating (Desolite 3471-3-14, DSM Desotech Inc.) was applied on-line during fiber drawing. The coating thickness represents ∼50% of the total fiber diameter and the polymeric material itself exhibits a tensile strength of about 12 MPa [25]; that is to say one order-of-magnitude lower than the glass As_2Se_3 and, therefore, bears a negligible portion of the load.

For this study eight preforms were prepared and drawn. They are labeled hereafter as 'a_i' (moisture removal), 'b_i' (oxides volatilization), 'c_i' (oxides volatilization + $AlCl_3$) and 'd_i' (oxides volatilization + $AlCl_3$ + distillation), with $i = 1$ for the uncoated fibers and $i = 2$ for the coated fibers (see Table 1).

3. Preforms and fibers characterization

3.1. Micro-hardness measurements

In order to evaluate the role of glass impurities on glass hardness, a Vickers micro-hardness was employed using a Shimadzu DUH-211S micro-hardness tester. The apparatus is composed of a square-base diamond pyramid with an apical angle of $136°$. A load of 200 mN was applied at a rate of 1.0 mN s^{-1} for a hold-time of 20 s. The diagonal length of the indentation was precisely measured on both bulk glass and uncoated fiber pieces using a light microscope connected to an imaging system and the micro-hardness value calculated. The bulk samples were cut directly from the preform and optically polished to remove mechanical strains or defects. In the case of the fibers, the diamond tip was applied in the longitudinal surface of the fibers. Two different diameters were tested for each type of fiber (150 and 200 μm). In order to minimize error in the measured hardness, values were averaged over 15 indentations per sample. Errors for micro-hardness measurements performed in this way are ±1%.

3.2. Infrared transmission

In order to quantify their impurity content the transmission spectrum of the as-prepared preforms were analyzed with Fourier Transform Infra-Red (FTIR) spectroscopy. A slice was cut from one end of the glass preform and subsequently polished to achieve mirror-like parallel faces, with a thickness of ∼2.0 mm. The transmission spectra of the glasses were measured using a Nicolet Magna-IR 560 FTIR spectrometer with a spectral resolution of 4 cm^{-1} and a dual beam Vis-NIR Perkin Elmer Lambda 900 spectrophotometer. Prior to transmission measurement the samples were placed in the spectrometer chamber and purged with nitrogen for 30 min.

3.3. Tensile measurements

Tensile tests measurements provide insight into the maximum uniaxial tensile strength that the fibers can sustain prior to fracture. These measurements were conducted using an Inston model 1125 apparatus, as shown in Fig. 2a. Fiber samples of approximately 6 cm in length were cut and held between two grips in a vertical position, with an initial distance L_0 = 30 mm between the two grips. Only the fibers that failed in their central portion were considered "valid measurements" in the data analysis (Fig. 2b). In order to help prevent the fibers ends from breaking or slipping within the clamps they were wrapped with thin cardboard pieces (as can be partially seen in Fig. 2b). For each test a computer recorded in real-time both the force, F, applied to the fiber and its resultant elongation, ΔL. The measurements were made on fibers with diameters ranging from 250 μm to 75 μm.

Table 1
Investigated As_2Se_3 fibers (a_i: moisture removal; b_i: oxide volatilization; c_i: oxide volatilization + $AlCl_3$; d_i: oxide volatilization + $AlCl_3$ + distillation; $i = 1$: uncoated; $i = 2$: coated).

Fiber	Purification	Coating
a_1	Moisture removal	NO
a_2	–	YES
b_1	Oxide volatilization	NO
b_2	–	YES
c_1	Oxide volatilization + $AlCl_3$	NO
c_2	–	YES
d_1	Oxide volatilization + $AlCl_3$ + distillation	NO
d_2	–	YES
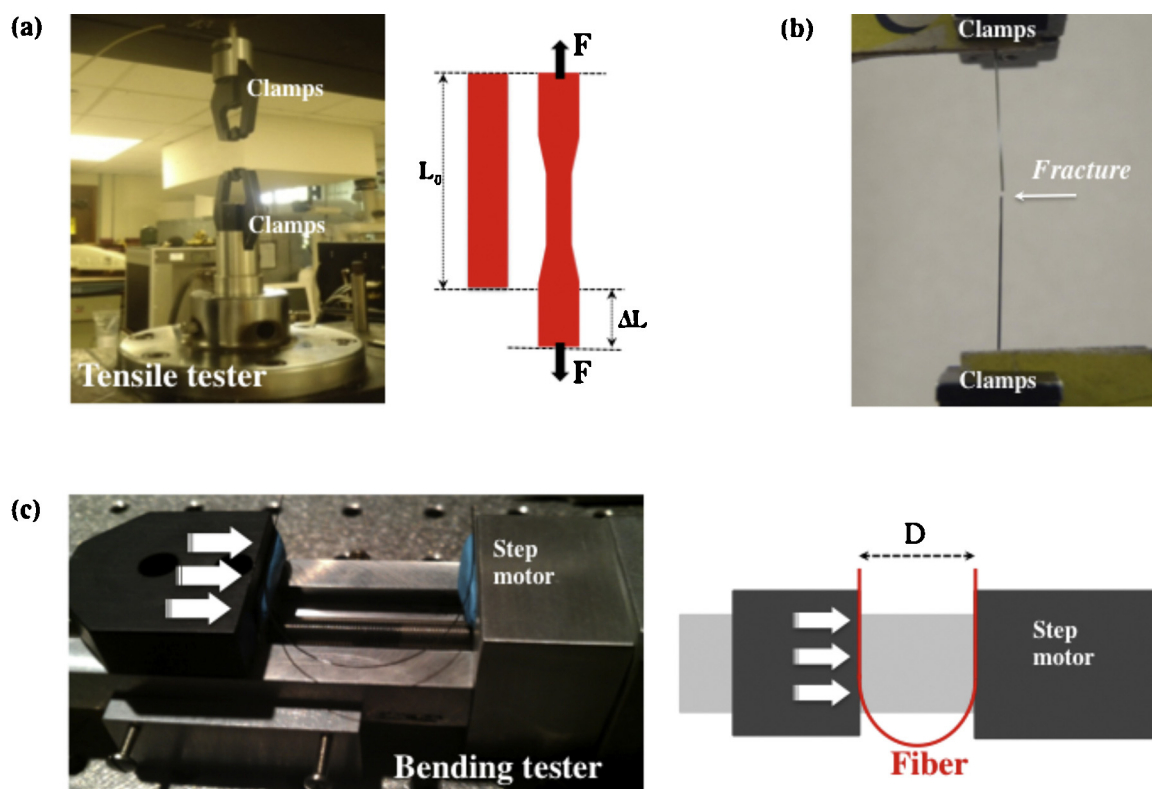
Fig. 2. (a) Instron model 1125 tensile apparatus and schematic of the measurement (b) Fiber breaking, counted as valid measurement (c) Two-point step-motor bending tester with scheme.

The tensile stress is given by dividing the load needed to fracture the fiber by the fiber's cross-sectional area. The modulus, E (Pa), is the proportionality constant between the applied tensile stress and the resulting strain, as shown in the equation (Eq. (1)) [26]:

$$E = \frac{\text{Stress}}{\text{Strain}} = \frac{\sigma}{\epsilon} = \frac{FL_0}{\Delta L A_0} \qquad (1)$$

with σ = tensile stress (Pa), ε = strain, F = force applied to the fiber under tension (N), L_0 = original length of fiber (m), A_0 = cross-section area of the fiber before the force is applied (m^2) and ΔL = change in length of the fiber due to the experiment (m). The Young's modulus was extracted for each fiber from the linear portion of the computed stress–strain curve. For Weibull statistics a minimum of 18 valid measurements were made per category of fiber. The gathered strength data were analyzed using Weibull statistics (see Section 4).

3.4. Bending measurements

The mechanical strength of the fiber can also be determined by two-point bending tests. The bending tester used in this study consists of a motorized-stage device in which a motor drove the faceplates at a controlled speed close to each other (Fig. 2c). This leads to the progressive bending of the fiber into an elliptical shape until the large tension concentrated at the fiber's apex eventually causes its failure. The maximum flexural stress, σ, of the fiber at rupture is calculated using the equation (Eq. (2)) [27]:

$$\sigma_{\max} = 1.198 \cdot E \cdot \frac{d_1}{D - d_2} \qquad (2)$$

with Young modulus, E, of the fiber (measured independently by tensile method), distance, D, at failure between the two plates,

diameter of the bare fiber, d_1, and overall diameter of the fiber, d_2 (including the coating). All measurements were carried out with ~10-cm-long sections, under standard temperature and humidity laboratory conditions, with a plate velocity of 0.5 mm/s. The distance D at which fiber failure occurs was recorded in real-time via a computer. The accuracy of the method was estimated to be ±2% for this apparatus. For each type of fiber the flexural strength was measured on a minimum of 35 specimens in order to obtain a meaningful number of data points. The collected strength data then was analyzed using Weibull statistics (see Section 4).

4. Results and discussion

Presented here is the influence of native preform purity on the resulting drawn fiber mechanical strength, with the goal of assessing purification protocols and the subsequent role of impurity content on these physical properties. Primary impurity contaminants in ChGs include oxygen, hydrogen, carbon or combinations of these species, as well as stable dissolved compounds and heterogeneous inclusions. After preparing preforms with specific purification protocols (see Table 1), the content of extrinsic impurity embedded within each was estimated. In all cases, purified preforms were compared to the properties of a reference (preform a_i) made using high-purity 5 N reagents. A glass slice of the preforms was cut and polished and its transmission spectrum analyzed using FTIR spectroscopy. The spectra are summarized in Fig. 3 (preforms drawn (a) without coating; and (b) with coating). The typical transparency in the IR region of the As$_2$Se$_3$ composition is observed with the multi-phonon cut-off edge being at ~20 μm and a maximum transmission at ~60% due to Fresnel reflections. The observed transparency discrepancies originate from sample's thickness and purification protocol variation.
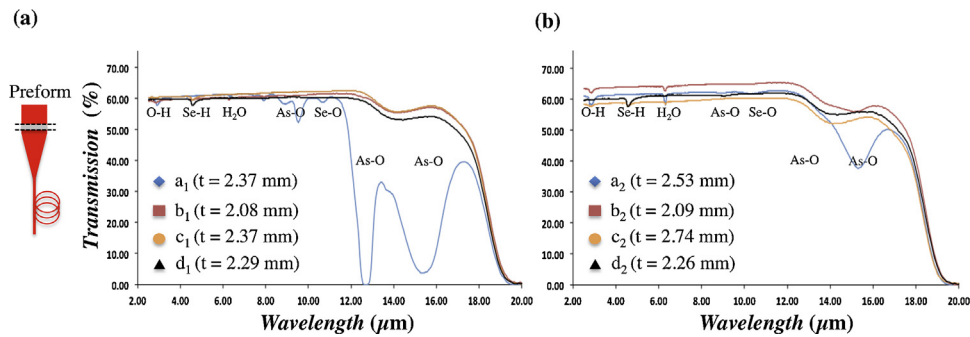
Fig. 3. Transmission spectrum of the As₂Se₃ preforms used for the drawing of (a) the uncoated fibers and of (b) the coated fibers.

The concentration of the impurity species contained in the preforms was extracted from the measured infrared transmission spectra using the following relation (Eq. (3)):

$$[\text{Impurities}] = \frac{\alpha}{\epsilon} \qquad (3)$$

with α the absorption coefficient (dB m^{-1}), and ε the extinction coefficient (dB m^{-1} ppm^{-1}) of a particular species of interest at a specific wavelength (hydrides: ε_{OH} = 5.0 dB m^{-1} ppm^{-1} at 2.92 μm [22], ε_{SeH} = 1.0 dB m^{-1} ppm^{-1} at 4.6 μm [22], and ϵ_{H_2O} = 34 dB · m^{-1} · ppm^{-1} [28], ε_{Se-O} = 0.38 dB m^{-1} ppm^{-1} at 10.60 μm [22]). The impurity concentrations calculated from Eq. (3) for H₂O, O–H, Se–H, and Se–O are summarized in Table 2. Arsenic oxide compounds exhibit a multiplicity of forms (As₄O₆, As₂O₃, As–O, As–O–As, As–O–H), which span in an intricate manner the 8–16 μm spectral range [29]. The extinction coefficients for these impurities species are only partially available ($\epsilon_{As_2O_3}$ = 1.03 dB m^{-1} ppm^{-1} at 9.50 μm [22], $\epsilon_{As_3O_3}$ = 43.0 dB m^{-1} ppm^{-1} at 12.65 μm [22]). In order to provide a more complete estimation of the evolution of the arsenic oxide impurities with the purification methods, Table 2 also includes the value of the absorption coefficient α calculated from the Fig. 3 results over the range 600–800 cm^{-1}.

With successive purification protocols (i.e., 'a' to 'b', 'c' and 'd'), two majors trends are observed in Table 2. Firstly, we note that, as compared with the protocol 'a', all of the three purification protocols 'b', 'c' and 'd' are very efficient at removing hydroxyls, molecular water and oxygen from the system. Indeed the concentration of O–H and H₂O groups consistently decrease, from a few tens-of-ppm for purification method 'a' to 0 ppm (i.e., below detection limit) for method 'd'. The Se–O species at 10.60 μm, as well as the arsenic oxide species at 9.50 μm and 12.65 μm, fall below the detection limit. Similarly the absorption coefficient α_{As-O} in the range 13–18 μm drops to ~0.50 cm^{-1}, that is to say the intrinsic minimum of the multi-phonon absorption of the glass As₂Se₃. As a drawback however we note a progressive bonding of the remaining elemental hydrogen to selenium as the oxygen is

progressively removed. It leads to a recurrent increase in the Se–H vibrational band centered on 4.57 μm (2175 cm^{-1}) to several tens-of-ppm, depending on the purification method. The current observation of impurity evolutions with purification protocols is in agreements with the author's previous work [23].

Micro-hardness testing provides important information on the resistance of a material to surface damage; in that respect the Vickers micro-hardness (VH) was measured on the uncoated fibers with diameters 150 and 200 μm ± 10 μm, and compared with values from their respective native bulk preforms (coated fibers were not tested since the coating can mask the intrinsic behavior of the glass). The results are summarized in Table 3, along with standard deviation and 95% confidence interval.

It is observed that the preform hardness increases, between ~1.5% ('d₁') and ~2% ('b₁'), as one goes from the moisture removal method to oxide volatilization, synthesis over getter and distillation, as corroborated by other recent observations [23]. The fiber's hardness, irrespective of the diameter, follows a similar trend with the purification method. For each purification method, the hardness of the fiber samples is larger than that of their corresponding preform. This result is in agreement with observation by Hach et al. [30]. Although an explanation of this phenomenon remains speculative, the draw-induced formation of a compressive glass layer and the alignment of the underlying glass structure are believed to contribute in the densification, and the associated hardness increase, of the glass fiber compare to its bulk analog.

A fiber can be viewed as a glass cylinder having an infinite length with a distribution of surface flaws. Therefore the strength of the fiber will be dictated by the most severe crack, that is to say where stress will be concentrated enough to cause catastrophic crack propagation. Weibull statistics often are used to give an indication of the variability of the fiber's strength resulting from a distribution of flaw sizes. Here the gathered tensile strength data were analyzed using Weibull statistics. According to a two-parameter Weibull model [26] the cumulative failure probability F

Table 2

Impurity concentrations in As₂Se₃ preforms as a function of purification method (0 ppm = below detection limit of the Fourier Transform Infra-Red spectrophotometer).

	Purification	Coating	Hydrides content (ppm)			Oxides content (ppm)			
			[O–H]	[Se–H]	[H₂O]	[Se–O]	[As–O]	[As–O]	α_{As-O} (cm^{-1})
			2.90 μm	4.6 μm	6.3 μm	10.6 μm	9.50 μm	12.65 μm	13–18 μm
a_1	Moisture removal	NO	13.10	0	0.53	100	210	370	>10.00
a_2	–	YES	17.31	0	2.95	30	10	1	2.00
b_1	Oxide volatilization	NO	4.26	10.50	0.82	0	0	0	0.50
b_2	–	YES	5.27	0	1.06	0	0	0	0.70
c_1	Oxide volatilization + AlCl₃	NO	0	35.14	0	0	0	0	0.45
c_2	–	YES	2.74	24.49	0.56	0	0	0	0.55
d_1	Oxide volatilization + AlCl₃ + distillation	NO	0	45	0	0	0	0	0.5
d_2	–	YES	0	88	0	0	0	0	0.5

Table 3
Vickers hardness with purification methods for As$_2$Se$_3$ preforms and fibers (STD: standard deviation; CI$_{95\%}$: 95% confidence interval).

	Purification	Preform			Fiber (150 μm ± 10 μm)			Fiber (200 μm ± 10 μm)		
		VH (GPa)	STD	CI$_{95\%}$	VH (GPa)	STD	CI$_{95\%}$	VH (GPa)	STD	CI$_{95\%}$
a_1	Moisture removal	1.40	0.030	1.396–1.404	1.45	0.04	1.445–1.455	1.44	0.04	1.435–1.445
b_1	Oxide volatilization	1.43	0.019	1.427–1.432	1.54	0.07	1.53–1.55	1.67	0.14	1.652–1.688
c_1	Oxide volatilization + AlCl$_3$	1.42	0.030	1.416–1.424	1.47	0.08	1.46–1.48	1.44	0.05	1.433–1.446
d_1	Oxide volatilization + AlCl$_3$ + distillation	1.42	0.019	1.417–1.423	1.52	0.14	1.502–1.538	1.55	0.14	1.532–1.568

as a function of a tensile stress x is given by the (Eq. (4)):

$$F(x) = 1 - e^{-(x/\lambda)^m} \qquad (4)$$

In Eq. (4), λ is a scale parameter (or 63% survival probability). The shape parameter, or Weibull modulus, m is a measure of scatter in the strength and is inversely related to the standard deviation. The cumulative probability of failure F_x was calculated by ranking values in ascending order where $F_x = (i - 0.3)/N + 0.4$, with N the total number of samples and i the ith data.

The derivation of Eq. (4) yields (Eq. (5)):

$$\ln\left(\ln\left(\frac{1}{1-F(x)}\right)\right) = m \cdot \ln(x) - m \cdot \ln(\lambda) \qquad (5)$$

The sorted data on a Weibull distribution are displayed by plotting Eq. (5), from which one can extract the scale (λ) and shape (m) parameters.

The tensile strength distribution of the investigated fibers as a function of the purification methods is depicted in Fig. 4 (panel a: uncoated; panel b: coated). All the calculations were made using Eq. (5) on a series of at least 18 valid measurements per category of fiber. It is expected that if the fiber's strength follows a Weibull distribution, the plotting of Eq. (5) yields fairly linear slopes, indicative of a homogenous population. Concerning uncoated fibers (Fig. 4a) this behavior is roughly respected for the samples a_1, b_1 and c_1, while the fiber d_1 yields two straight-line sections, indicative of a bi-modal distribution of flaws. None of the coated fibers (Fig. 4b) yields straight-lines, but rather tri-modal (a_2 to c_2) or bimodal (d_2) Weibull distribution. Table 4 summarizes the average fracture stress in tensile, and parameters λ and m, as a function of purification methods for the uncoated and coated fibers. The average stress (and associated standard deviation and 95% confidence interval), is calculated for each fiber on the whole set of data points. As can be seen in Fig. 4, Weibull probability plots are not all truly linear but are better described as fragmented segments (noted (i)–(iii)). The parameters λ and m are then extrapolated by finding the best-fit straight line for each of these segments.

Considering the uncoated fibers, the oxide volatilization thermal treatment favors the fiber's strength since the average tensile stress increases by about 40% from 93.6 MPa (a_1) to 131.3 MPa (b_1); this positive influence of oxide volatilization purification is consistently observed, both in tensile and in bending, for coated and uncoated fibers. When AlCl$_3$ getter is added to the glass batch without subsequent distillation (c_1) the tensile stress decreases to 83.6 MPa; the detrimental impact of this method of purification will be further observed over this study. Finally the complete purification protocol, involving oxide volatilization, and synthesis over getter followed by static distillation (d_1) leads to an increase of the average tensile stress of nearly 50% from 83.6 (c_1) to 125.0 MPa; the beneficial influence of the later purification method on fiber strength is consistently observed. If one considers coated fibers, the oxide volatilization purification increases the average tensile stress, from 138.0 MPa (a_2) to 157.8 MPa (b_2). When AlCl$_3$ getter is added to the melt without subsequent distillation (c_2) the tensile stress decreases to 119.6 MPa. Finally the purification protocol involving oxide volatilization, synthesis over getter and static distillation (d_2) leads to an increase of the average tensile stress, from 119.6 (c_2) 177.7 MPa. The strength of fibers depends on multiple factors (drawing parameters, storage condition, handling), which make direct comparison challenging. However, with such restriction in mind, we note that our tensile strength values are in good agreements with those results reported in a previous study [13]. As is shown in Fig. 4, statistical tensile distributions tend to deviate from a perfectly linear Weibull model. As a consequence the parameters λ and m, calculated for each segment, can spread strongly on a same distribution. Yet, if one excepts noticeable deviations (segments a_2(i), b_2(ii), c_2(ii)), the modulus m remains close to the range 5–15 usually observed for glasses [26].

Similarly the bending strength distribution of the fibers a_i to d_i ($i = 1, 2$) is plotted in Fig. 5 as a function of the purification methods (panel a: uncoated; panel b: coated). All the calculations were made using Eq. (5) on series of at least 35 valid measurements per
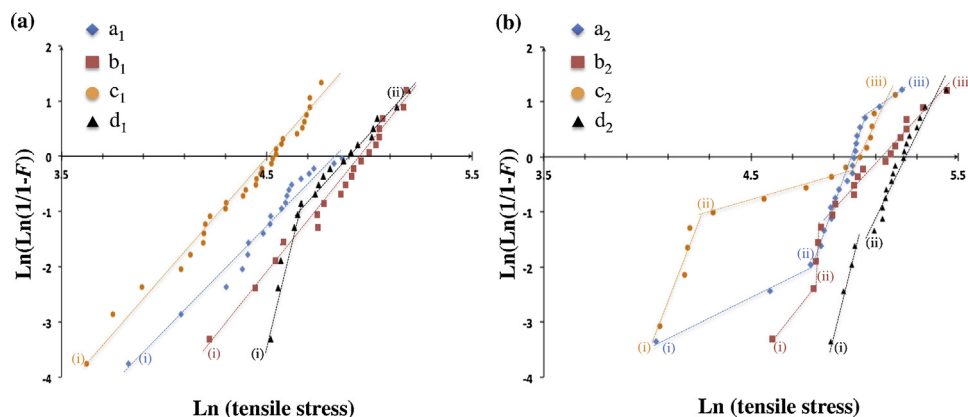
Fig. 4. Weibull distribution of the tensile strength with purification method for (a) uncoated and (b) coated fibers.

Table 4

Average tensile fracture stress, median fiber strength and Weibull modulus for (*left*) uncoated and (*right*) coated fibers (STD: standard deviation, $CI_{95\%}$: 95% confidence interval).

Tensile		Uncoated					Coated				
Purification		<Fracture stress> (Mpa)	STD	$CI_{95\%}$	λ (Mpa)	m		<Fracture stress> (Mpa)	STD	$CI_{95\%}$	λ (Mpa)	m
Moisture removal	a_1	93 6	20.7	91.6–95.6	(i) 123.6	4.0	a_2	138.0	26.3	135.4–140.6	(i) 358.0 (ii) 147.5 (iii) 122.4	1.8 9.8 2.9
Oxides volatilization	b_1	131.3	30.1	128.3–134.3	(i) 143.5	4.5	b_2	157.8	34.3	154.4–161.2	(i) 204.7 (ii) 130.8 (iii) 167.8	4.6 31.6 4.1
Oxides volatilization + $AlCl_3$	c_1	83.6	21.2	81.5–85.7	(i) 92.0	4.1	c_2	119.6	44.0	115.3–123.9	(i) 76.9 (ii) 163.2 (iii) 150.6	11.1 1.4 6.8
Oxides volatilization + $AlCl_3$ + distillation	d_1	125.0	26.4	122.4–127.6	(i) 111.6 (ii) 133.1	14.5 3.8	d_2	177.7	24.3	175.3–180.1	(i) 166.1 (ii) 189.0	14.8 7.9

category of fiber. As shown in Fig. 5a, only the uncoated fiber c_1 exhibits a linear Weibull distribution, indicative of a homogenous population of flaws. The additional fibers present bi-modal (a_1) or tri-modal (b_1 and d_1) distribution. None of the coated fibers (Fig. 5b) yields straight-lines, but rather bi-modal (a_2 to c_2) or tri-modal (d_2) Weibull distribution. Table 5 summarizes the average fracture stress in bending (and associated standard deviation and 95% confidence interval) calculated on the whole set of data, median fiber strength λ and Weibull modulus m as a function of purification methods for the uncoated and coated fibers. In the situation where the Weibull plots are better described as fragmented segments (noted (i)–(iii)), the parameters λ and m are calculated from a linear fit of these segments.

The oxide volatilization thermal treatment clearly enhanced the bending strength of uncoated fibers, with the average stress increasing from 98.0 MPa (a_1) to 128.3 MPa (b_1). When $AlCl_3$ getter is added to the melt without subsequent distillation (c_1) the bending stress decreases to 88.6 MPa. The complete purification protocol (d_1) leads to an increase of the average stress, from 88.6 (c_1) to 137.2 MPa. If one considers the coated fibers the oxide volatilization enhances the average bending stress, from 170.0 MPa (a_2) to 190.7 MPa (b_2). When $AlCl_3$ getter is added to the melt without subsequent distillation (c_2) the stress decreases to 110.2 MPa. Finally the purification protocol 'd_2' leads to an increase of the average bending stress to 201.6 MPa. Similar to tensile measurements, one observes in Fig. 5 that the bending distributions tend to deviate from a perfectly linear Weibull model. Yet, again, if one excepts discernible deviations (segments b_1(i), d_1(i) and (iii), c_2(ii)), the modulus m remains close to the range 5–15.

The sources of failure in fibers encompass multiple factors, such as micro- and/or macro-bubbles, dust or micro-cracks, which can severely mask or alter the sole effect of extrinsic impurities on fiber breaking behavior. Furthermore it can lead to a multi-modal distribution of flaws as observed above (Figs. 4 and 5). Nevertheless, despite these limitations, the effect of the purification methods on the fiber strength displays consistent trends, both in tensile (Table 4) and in bending (Table 5) strength. First, one observes that the preforms purified via surface oxide volatilization by thermal treatment of their reagents (b_i) lead to fibers with higher strength, both in tension and in bending, as compare to the reference fibers purified by moisture removal (a_i). Churbanov et al. [31,32] have shown in the As_2Se_3 glass that for thermo-dynamic reasons (As–O bond is notably stronger than the Se–O bond, ~480 kJ mol^{-1} versus ~420 kJ mol^{-1} respectively) oxygen impurities are more likely to combine with As_2 and As_4 molecules rather than with Se_n chains to form polymer made by $AsO_{3/2}$ structural units. Ultimately it forms inclusions (crystalline claudetite As_2O_3 and As_4O_6 cells molecules) in the process of melt solidification. As shown in Table 2, oxide volatilization strongly lower the amount of oxygen, and to a lesser extent of the hydrides, contained in the glass system, leading to a reduction in the content of arsenic oxide inclusions; we believe this effect is accountable in the improvement observed on the micro-hardness of the preform (Table 3). As fiber processing can exacerbate the nucleation and growth of scattering centers, having fewer inclusions in the preform leads ultimately to fiber with higher mechanical property ($b_{1,2}$ as compared to $a_{1,2}$). The fibers purified via oxide volatilization combined with $AlCl_3$ getter (c_i) do not exhibit similar improvement of their resistant to constraint. Although this method is very
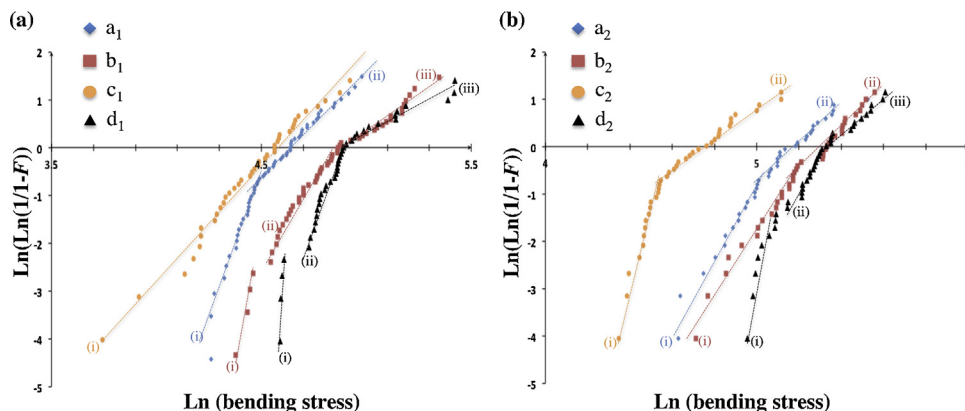
Fig. 5. Weibull distribution of the bending strength with purification method for (a) uncoated and (b) coated fibers.

Table 5
Average bending fracture stress, median fiber strength and Weibull modulus for (*left*) uncoated and (*right*) coated fibers (STD: standard deviation, $CI_{95\%}$: 95% confidence interval).

Bending		Uncoated					Coated				
Purification		<Fracture stress> (Mpa)	STD	$CI_{95\%}$	λ (Mpa)	m	<Fracture stress> (Mpa)	STD	$CI_{95\%}$	λ (Mpa)	m
Moisture removal	a_1	98.0	18.0	97.1–98.9	(i) 92.7 (ii) 103.2	13.6 4.4	a_2 170.0	44.9	167.8–172.2	(i) 171 (ii) 174.9	7.1 3.2
Oxides volatilization	b_1	128.3	31.0	126.8–129.8	(i) 98.7 (ii) 129.3 (iii) 133.5	20.1 6.5 3.2	b_2 157.8	42.2	188.6–192.7	(i) 194.7 (ii) 206.4	6.7 4.9
Oxides volatilization + AlCl$_3$	c_1	88.6	20.6	87.6–89.6	(i) 96.5	4.9	c_2 119.6	25.3	109.0–111.0	(i) 97.9 (ii) 115.3	16.0 3.3
Oxides volatilization + AlCl$_3$ + distillation	d_1	137.2	31.5	135.7–1387	(i) 103 (ii) 133.2 (iii) 135.0	86.1 11.1 2.1	d_2 177.7	42.7	199.5–203.7	(i) 178.1 (ii) 205.1 (iii) 217.9	15.5 8.1 4.4

efficient at eliminating hydroxyls, water and oxides from the system (Table 2), it generates refractory alumina Al_2O_3 as a by-product of the reaction between the aluminum and the oxygen impurities [22]. Alumina, with a melting point ($T_m = 2072\ °C$) well above the glass and fiber processing temperatures, will remain within the preform and fiber glassy matrix. Its presence will behave as a crystallite nucleating site during fiberization, to ultimately alter the fibers thermo-mechanical properties. When an additional distillation step is added to the preforms purification (d_i) the fibers strengths revert back to values similar or superior to the ones prepared via oxide volatilization (b_i). The purification method 'd' purposely aims at efficiently lowering the content of oxygen impurity (therefore the content of arsenic oxide inclusions) from the batch but also of refractory alumina compounds. The removal of extrinsic impurities produces preforms with fewer structural defects, so to fibers with fewer flaws; as a consequence the fiber strength increases (d_i as compared to a_i, b_i, c_i).

Noteworthy, the evolution with purification of the average fiber strengths and of the glass hardness (preforms and fibers; Table 3) follows a similar trend. Indeed both quantities, fracture stress and hardness, increase as one progresses from purification method a_i to b_i, then decreases with method c_i to finally increasing again (d_i). Discrepancies in ChGs-based fiber strength emanate not only from difference in glass crack growth resistance but in severity of flaws as well [17]. Nevertheless this result shows that the toughness of a material, which dictates the ability of the solid to resist initiation and propagation of surface flaws or cracks through the bulk, still play a major role in the resulting strength of the fiber.

If one compares the fracture stress for the uncoated versus coated fibers in tension (Table 4) and in bending (Table 5), irrespective of the purification method, we observe an increase in all stress values by about 40%. Uncoated fiber surfaces can bear remnants of the manufacturing processing, storage and environment conditions. Consequently, they manifest themselves with larger propagation of cracks on the surface, impurity absorption, or microstructural changes, all of which contributing to a reduction in the overall fiber robustness. It is therefore expected that coated fibers, having their surface protected from abrasion and chemical damage, exhibit improved mechanical properties. Furthermore the soundness of this study of fiber strength with purification method is reinforced further by the correlation observed between uncoated and coated fibers. Indeed it allows deconvolution of the source of the external fiber's degradation, such as manufacturing, handling or aging, from the actual strength measurements. In tensile (Fig. 4) and in bending (Fig. 5), the Weibull distributions deviate from a linear model, which suggests a non-uniform distribution of flaws at the surface

of the fibers. However this scatter in the data is true both for uncoated and coated fibers. Glass fiber strength is not only vastly dictated by surface flaws but by bulk defects as well, such as bubbles. Fractographic analyses [17,33] has proven itself a successful method to provide fruitful insight into the fracture's origin and will be the focus of further investigation to better assess the fiber breaking mechanisms.

Explored here was how native As_2Se_3 preform impurity level impacts the maximum stress of the resulting glass optical fibers. It is expected that direct improvements to fiber strength will be realized via improvement in the purity of the constituent materials. Hence further optimizations are in progress to refine the synthesis procedures presented here. Special attention will be paid to the removal of residual hydrides impurities by more aggressive getters and/or by multiple distillations. As an alternative purification route, the authors have recently demonstrated the fabrication of ChGs via microwave heating with level of hydrides and oxides impurity equal to or lower than those available in commercial glasses [34]. In addition to purification efforts, the fabrication of high-strength fibers necessitates a critical attention paid to details during preform and fiber manufacturing, not only to reduce the propagation of flaws, but, most of all, to reduce the probability of their generation in the first place.

5. Conclusion

The engineering of low-loss mechanically-robust ChGs optical fiber is of technological importance. In this study, for the first time to our knowledge, a systematic investigation of the correlation between fiber mechanical robustness and native preform impurity level has been carried out. Irrespective of the eventual presence of a coating, the fiber's tensile and bending strength is shown to relate to the method of preform purification. Oxide volatilization thermal treatment enables producing preforms with fewer inclusions, so to fibers with higher mechanical strength. Furthermore, the detrimental effect of $AlCl_3$ getter on the fiber mechanical properties is amplified when the remaining by-product of its reaction with the oxygen impurities, i.e., Al_2O_3 compound, is not removed from the glass batch by static distillation. If further distillation of the preform is carried out the fiber's strength improves slightly in comparison to oxide volatilization treatment. As expected, additional protective coating yields an increase in the fiber's strength. Most of all uncoated and coated fibers show similar trends in their strength with respect to purification methods. Future works will consist of refining preforms purification protocols to eliminate residual hydride compounds further and to correlate this improvement with the fibers mechanical properties.

Acknowledgments

References

[1] N.S. Kapany, R.J. Simms, Infrared Phys. 5 (1965) 69–76.
[2] J.D. Shephard, W.N. MacPherson, R.R.J. Maier, J.D.C. Jones, D.P. Hand, M. Mohebbi, A.K. George, P.J. Roberts, J.C. Knight, Opt. Express 13 (2005) 7139–7144.
[3] T.D. Engeness, M. Ibanescu, S.G. Johnson, O. Weisberg, M. Skorobogatiy, S. Jacobs, Y. Fink, Opt. Express 11 (2003) 1175–1196.
[4] I. Savelii, O. Mouawad, J. Fatome, B. Kibler, F. Désévédavy, G. Gadret, J.-C. Jules, P.-Y. Bony, H. Kawashima, W. Gao, T. Kohoutek, T. Suzuki, Y. Ohishi, F. Smektala, Opt. Express 20 (2012) 27083–27093.
[5] Z. Wang, N. Chocat, Curr. Pharm. Biotechnol. 11 (2010) 384–397.
[6] M. Asobe, T. Ohara, I. Yokohama, T. Kaino, Electron. Lett. 32 (1996) 1396–1397.
[7] R.E. Slusher, G. Lenz, J. Hodelin, J. Sanghera, L.B. Shaw, I.D. Aggarwal, J. Opt. Soc. Am. B 21 (2004) 1146–1155.
[8] T. Kohoutek, X. Yan, T.W. Shiosaka, S.N. Yannopoulos, A. Chrissanthopoulos, T. Suzuki, Y. Ohishi, J. Opt. Soc. Am. B 28 (2011) 2284–2290.
[9] B. Bureau, X.H. Zhang, F. Smektala, J.L. Adam, J. Troles, H.L. Ma, C. Boussard-Pledel, J. Lucas, P. Lucas, D. Le Coq, M.R. Riley, J.H. Simmons, J. Non-Cryst. Solids 345 (2004) 276–283.
[10] W. Weibull, Handlingar, Royal Swedish Acad. Energy Sci. 151 (1939) 1–45.
[11] Y. Paramonov, J. Andersons, Composites: Part A 38 (2007) 1227–1233.
[12] D.J. McEnroe, W.C. LaCourse, J. Am. Ceram. Soc. 72 (1989) 1491–1494.
[13] S.H. Shieh, W.C. LaCourse, Mater. Chem. Phys. 35 (1993) 21–27.
[14] S.H. Shieh, Ph.D. Theses, Alfred University, 1987.
[15] M.F. Churbanov, V.S. Shiryaev, V.V. Gerasimenko, A.A. Pushkin, I.V. Skripachev, G.E. Snopatin, V.G. Plotnichenko, Inorg. Mater. 38 (2002) 1063–1068.
[16] C. Pouvreau, M. Drissi-Habti, K. Michel, B. Bureau, J.C. Sangleboeuf, C. Boussard-Pledel, T. Rouxel, J.L. Adam, J. Non-Cryst. Solids 316 (2003) 131–137.
[17] J.B. Quinn, V.Q. Nguyen, J.S. Sanghera, I.K. Lloyd, P.C. Pureza, R.E. Miklos, I.D. Aggarwal, J. Non-Cryst. Solids 325 (2003) 150–157.
[18] V.S. Shiryaev, L.A. Ketkova, M.F. Churbanov, A.M. Potapov, J. Troles, P. Houizot, J.L. Adam, A.A. Sibirkin, J. Non-Cryst. Solids 355 (2009) 2640–2646.
[19] M.F. Churbanov, G.E. Snopatin, V.S. Shiryaev, V.G. Plotnichenko, E.M. Dianov, J. Non-Cryst. Solids 357 (2011) 2352–2357.
[20] A.W. King, A.G. Clare, W.C. LaCourse, J. Non-Cryst. Solids 181 (1995) 231–237.
[21] M.F. Churbanov, J. Non-Cryst. Solids 184 (1995) 25–29.
[22] G.E. Snopatin, V.S. Shiryaev, V.G. Plotnichenko, E.M. Dianov, M.F. Churbanov, Inorg. Mater. 45 (2009) 1439–1460.
[23] S. Danto, B. Giroire, D. Thompson, P. Wachtel, J.D. Musgraves, K. Richardson, Int. J. Appl. Glass Sci. 4 (2013) 31–41.
[24] E.M. Dianov, V.G. Plotnichenko, G.G. Devyatykh, M.F. Churbanov, I.V. Scripachev, Infrared Phys. 29 (1989) 303–307.
[25] Technical, Technical Datasheet on Desolite Website, 2012 (accessed on 11.28.12, http://www.dsm.com/en_US/supercoatings/public/home/pages/homepage.jsp).
[26] A.K. Varshneya, Fundamental of Inorganic Glasses, 2nd ed., Society of Glass Technology, Academic Press, London, UK, 1994.
[27] M.J. Matthewson, C.R. Kurkjian, S.T. Gulati, J. Am. Ceram. Soc. 69 (1986) 815–821.
[28] F.M. Ernsberger, J. Am. Ceram. Soc. 60 (1977) 91–92.
[29] C.T. Moynihan, P.B. Macedo, M.S. Maklad, R.K. Mohr, R.E. Howard, J. Non-Cryst. Solids 17 (1975) 369–385.
[30] C.T. Hach, K.C. Richardson, J.R. Varner, W.C. LaCourse, J. Non-Cryst. Solids 209 (1997) 159–165.
[31] M.F. Churbanov, I.V. Scripachev, G.E. Snopatin, V.S. Shiryaev, V.G. Plotnichenko, J. Optoelecron. Adv. Mater. 3 (2001) 341–349.
[32] M.F. Churbanov, V.S. Shiryaev, S.V. Smetanin, V.G. Pimenov, E.A. Zaitseva, E.B. Kryukova, V.G. Plotnichenko, Inorg. Mater. 37 (2001) 1188–1194.
[33] T.E. Easler, R.C. Bradt, R.E. Tressler, J. Am. Ceram. Soc. 64 (1981) 53–55.
[34] D. Thompson, S. Danto, J.D. Musgraves, P. Wachtel, B. Giroire, K. Richardson, Phys. Chem. Glasses: Eur. J. Glass Sci. Technol. B 54 (2013) 27–34.